proceedings

Abstract

Determining the Defect Sizes of CFRP Laminates by Employing Step-heating Thermography and an Artificial Neural Network Approach†

Muhamad Hidayat [1], Yishuo Huang [2] and Chih-Hung Chiang [3,*]

[1] Department of Mechanical Engineering, Sumbawa University of Technology, Sumbawa, West Nusa Tenggara, 84371, Indonesia; muhamad.hidayat@uts.ac.id
[2] Department of Civil and Construction Engineering, Chaoyang University of Technology, Taichung City 413310, Taiwan; yishuoh@gmail.com
[3] Center for NDT and Graduate Institute of Aeronautics, Chaoyang University of Technology, Taichung City 413310, Taiwan; chiangc@cyut.edu.tw
* Correspondence: chiangc@cyut.edu.tw
† Presented at the "Advanced Infrared Technology and Application (AITA)" in Kobe, Japan, on 15-19 September 2025

Keywords: step-heating thermography; image segmentation; artificial neural net

1. Introduction

Components and structures made from composite materials can develop defects at various stages, including during manufacturing [1] and as a result of in-service use [2]. These issues can manifest as impact damage, internal flaws like resin or transverse ply cracks, voids, porosity, and poorly bonded interlaminar regions [3], often stemming from production errors. Such defects compromise the structural integrity and reduce the strength of the component.

While surface defects are readily observable, internal defects pose a greater challenge for detection. Traditional inspection methods often lack the effectiveness to identify these subsurface flaws, highlighting the need for more sophisticated non-destructive testing (NDT) techniques. Thermography testing (TNDT) has emerged as one of the promising NDT methods for detecting defects within Carbon Fiber Reinforced Polymer (CFRP) structures.

Experimental methods for defect detection often require substantial time and financial resources. To address these limitations, simulation-based approaches have been increasingly adopted. In particular, simulation-based TNDT has proven effective for identifying internal defects in CFRP composites [4].

Defect size in materials can be measured using methods like Full-Width Half Maximum (FWHM) [5], temperature profile derivatives [6], and machine learning [7]. This study explores this problem using a combined methodology.

Deep learning is widely used in defect detection. This study leverages deep learning to explore the relationship between thermal images—capturing surface temperatures of CFRP samples—and FEA-simulated images. A Generative Adversarial Network (GAN) was developed to train the data and generate simulations closely matching the originals.

2. Model and Specimen

The simulation model and experimental specimen were both constructed from woven rectangular CFRP prepreg, comprising seven layers with a stacking sequence of

Citation: To be added by editorial staff during production.

Academic Editor: Firstname Lastname

Published: date

[+45/0/-45/0/-45/0/+45]. Each layer had a nominal thickness of 0.28 mm. However, the overall thicknesses differed: the model had a thickness of 1.96 mm, while the manufactured specimen measured 1.89 mm, likely due to thickness shrinkage during the fabrication process. The dimensions and defect layout are detailed in Figure 1. Two types of defects have been analyzed: void defects (1A, 1B, 1C) and polyethylene defects (2A, 2B, 2C).

Specimen material thermal conductivity values were based on Joven's research [8] for Cytec T300 3k/977-2 plain weave, with additional data for Cytec T300 sourced from Toray [9]. Material properties are listed in Table 1.

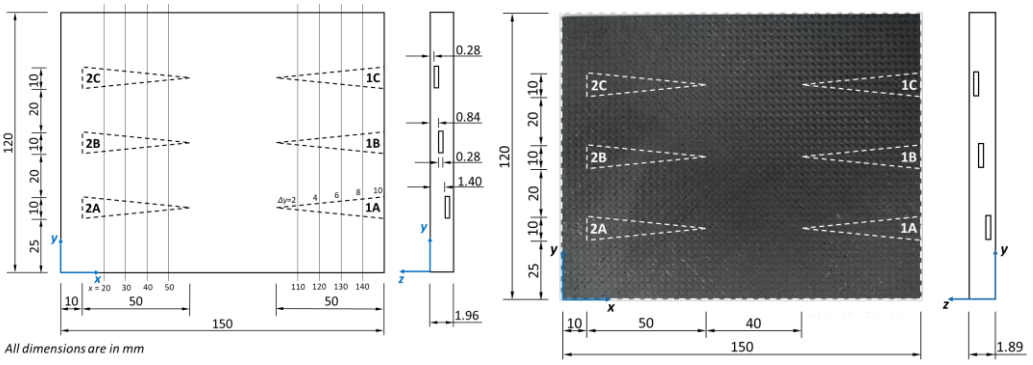

(a) (b)

Figure 1. Dimension and defect layout: (a) Model and (b) experiment.

Table 1. Material's properties.

Material	Thermal Conductivity [1]			Specific Heat [2]	Density [3]
	x	y	Z		
Woven CFRP Prepeg	3.1	3.1	0.6	1000	1420
Polyethylene	-	0.28	-	2300	950
Void (air)	-	0.026	-	1021	1.13

[1] Thermal Conductivity in W/m.K; [2] Specific Heat in J/kg.K; [3] Density in kg/m^3

Finite Element Analysis

The mesh model, constructed with SOLID278 and SURF152 elements, used a 0.25 mm mesh size, chosen to approximate the 0.36 mm pixel size of the experiment. Natural cooling of the model was simulated with convective heat transfer (h = 5 W/m^2.K) occurring at all surfaces. The ambient temperature was 26.5 ^{o}C, and the data acquisition rate was 3 Hz. Two analyses were carried out. The first applied a uniform heat flux of 650 W/m^2 to the front surface for 21s. The second analysis applied a uniform heat flux of 925 W/m^2 to the back surface for 30s.

Experimental Design

Two identical 500W halogen lamps provided the heat source. The lamps heat the specimen surface for about 34 seconds for the front heating and 37 seconds for the back heating. An infrared camera, Avio InfRec R500EX, captured the thermal images and provide the thermal data. The camera acquisition rate was set at 3 Hz for 120 seconds. The room temperature was 25 ^{o}C.

3. Defect Size Determination

The defect size measured along the y-axis at position x = 20, 30, 40, and 50 mm for polyethylene defects, and x = 140, 130, 120, and 110 mm for void defects, correspond to defect widths (Δy) of 8, 6, 4, and 2 mm, respectively, as shown in Figure 1(a).

Defect size was quantified using two methods: Full-Width Half Maximum (FWHM) and the derivative of the temperature profile. FWHM measures the width at half the

maximum temperature contrast. The derivative method measures the distance between the peaks of the temperature profile's first derivative around the defect, a technique linked to maximum lateral heat fluxes at defect border projections [6].

4. Result

Measurement error comparisons of the front and back heating simulation and experiments are tabulated in Tables 2 and 3. In evaluating defect detectability using front heating:

1. The simulation identified minimum detectable defect sizes of 6 mm (derivative) for polyethylene and 4 mm (FWHM and derivative) for void defects.
2. Conversely, the experiment did not detect polyethylene defects, while it detected void defects with a minimum size of 6 mm (derivative).

For back heating:

3. The simulation achieved a minimum detectable defect size of 4 mm (derivative) for both polyethylene and void defects (FWHM and derivative).
4. The experiment detected polyethylene defects at a minimum size of 8 mm (FWHM) and void defects at 4 mm (derivative).

Table 2. Measurement error for the front heating.

Defect	Size	Simulation		Experiment	
		FWHM	Derivative	FWHM	Derivative
Polyethylene	8 mm	27%	12%	24%	33%
	6 mm	43%	13%	65%	72%
	4 mm	76%	22%	113%	-
Void	8 mm	14%	11%	7%	9%
	6 mm	27%	10%	15%	8%
	4 mm	60%	16%	35%	67%

Table 3. Measurement error for the back heating.

Defect	Size	Simulation		Experiment	
		FWHM	Derivative	FWHM	Derivative
Polyethylene	8 mm	26%	7%	19%	29%
	6 mm	55%	8%	36%	64%
	4 mm	95%	16%	-	-
Void	8 mm	16%	17%	27%	20%
	6 mm	11%	11%	18%	11%
	4 mm	13%	15%	43%	7%

5. Discussion

Perfect alignment between infrared thermal and FEA-simulated images is difficult to obtain. However, the simulated results are difficult to distinguish from the discriminators those provided by GAN. CycleGAN addresses this by learning to translate between the two image domains without requiring paired data [10].

In this study, we leverage the CycleGAN model to learn the translation between collected infrared thermal images and FEA simulated images. The 2000 iterations can reach the convergence. The differences between Generator G and F are decreasing as the

iterations increase. Furthermore, the differences between the discriminators X and Y can decrease after 2000 iterations, as shown in Figure 2.

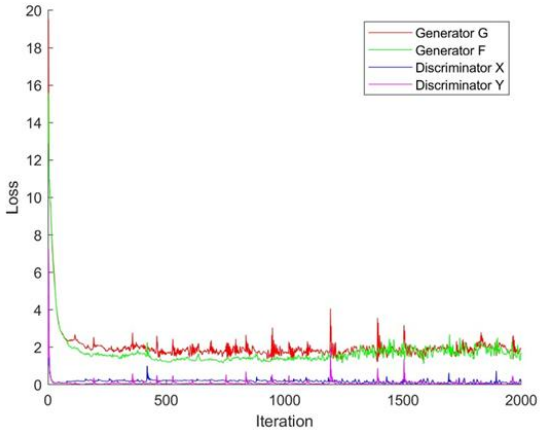

Figure 2. The relations of the loss functions and generators G and F and the discriminators X and Y

6. Conclusion

Two main conclusions can be drawn based on the results of the current study:

1. For estimating defect size, the derivative method demonstrated good performance in the simulation, whereas the FWHM method yielded better results in the experiment.
2. Further refinement of the CycleGAN model is necessary before it can be reliably used for defect predictions.

Author Contributions: Conceptualization and methodology: M.H. and C.C.; software, validation, formal analysis, data curation, visualization, and investigation: M.H. and Y.H.; Writing—original draft preparation, M.H.; writing—review and editing: M.H., Y.H., and C.C.; project administration, and funding acquisition: C.C.

Funding: This work was supported by NSTC, Taiwan. Project number NSTC 113-2221-E-324-005.

Conflicts of Interest: The authors declare there are no conflicts of interest.

References

1. Almeida, J.H.S.; Angrizani, C.C.; Botelho, E.C.; Amico, S.C. Effect of Fiber Orientation on the Shear Behavior of Glass Fiber/Epoxy Composites. *Mater. Des. 1980-2015* **2015**, *65*, 789–795, doi:10.1016/j.matdes.2014.10.003.
2. Rao, K.S.; Varadarajan, Y.S.; Rajendra, N. Erosive Wear Behaviour of Carbon Fiber-Reinforced Epoxy Composite. *Mater. Today Proc.* **2015**, *2*, 2975–2983, doi:10.1016/j.matpr.2015.07.280.
3. Nsengiyumva, W.; Zhong, S.; Lin, J.; Zhang, Q.; Zhong, J.; Huang, Y. Advances, Limitations and Prospects of Nondestructive Testing and Evaluation of Thick Composites and Sandwich Structures: A State-of-the-Art Review. *Compos. Struct.* **2021**, *256*, 112951, doi:10.1016/j.compstruct.2020.112951.
4. Hidayat, M.; Chiang, C.-H.; Yen, M. Determination of the Defect's Size of Multi-Layer Woven CFRP Based on Its Temperature Profile. *Int. J. Appl. Sci. Eng.* **2023**, *20*, 1–9, doi:10.6703/IJASE.202309_20(3).003.
5. Guo, W.; Dong, L.; Wang, H.; Feng, F.; Xing, Z.; Ma, R.; Shao, H.; Gao, Z.; Wang, B.; Yang, J. Size Estimation of Coating Disbonds Using the First Derivative Images in Pulsed Thermography. *Infrared Phys. Technol.* **2020**, *104*, 103106, doi:10.1016/j.infrared.2019.103106.
6. Vavilov, V.P. 3D Modeling of Pulsed Thermal NDT: Back to Basic Features and Subtle Phenomena. *NDT E Int.* **2022**, *130*, 102659, doi:10.1016/j.ndteint.2022.102659.
7. Daghigh, V., Ramezani, S.B., Daghigh, H., Lacy, T., Explainable artificial intelligence prediction of defect characterization in composite materials. *Composites Science and Technology*, **2024**, 256, 110759, doi: 0.1016/j.compscitech.2024.110759.
8. Joven, R.; Das, R.; Ahmed, A.; Roozbehjavan, P.; Minaie, B. THERMAL PROPERTIES OF CARBON FIBER-EPOXY COMPOSITES WITH DIFFERENT FABRIC WEAVES.
9. Carbon Fiber and Prepreg Data Sheets | Toray Composite Materials America. *Toray Compos. Mater. Am. Inc*.
10. Zhu, Y.-H., Park, T., Isola, P., Efros, A. A. Unpaired Image-to-Image Translation Using Cycle-Consistent Adversarial Networks. IEEE International Conference on Computer Vision (ICCV), Venice, Italy, 2017, 2242-2251, doi: 10.1109/ICCV.2017.244.